International Journal on Interactive Design and Manufacturing (IJIDeM)
https://doi.org/10.1007/s12008-025-02436-x

ORIGINAL ARTICLE

Hot workability behaviour of AISI304 stainless steel: constitutive and ANN modelling

Japheth Obiko[1] · **Brendon Mxolisi**[1] · **Malatji Nicholus**[1]

Received: 9 June 2025 / Revised: 26 August 2025 / Accepted: 23 October 2025

Abstract

This article reports on the findings obtained from the hot deformation behaviour of AISI 304 stainless steel. Uniaxial compression tests were done using the Gleeble® thermal mechanical equipment. The test conditions were a deformation temperature range of 950–1050°C and a strain rate range of 0.1–15 s^{-1}. The study analysed the metal flow pattern and compared the prediction accuracy of the Arrhenius, strain-compensation, and physical and Artificial Neural Networks (ANN) models using statistical parameters: the correlation coefficient *R* and average absolute relative error *AARE*. The results show that flow stress increases with a decrease in the deformation temperature and an increase in strain rate, and vice versa. The predicted data obtained using the ANN model accurately tracks the experimental data throughout the entire loading condition range. However, the constitutive model analyses show a marked deviation from experimental data. The statistical parameters *R* and *AARE* analysis were: the *R*-values 0.994 (Arrhenius), 0.994 (strain compensated), 0.980 (Physical model) and 0.998 (ANN), and the *AARE*-values 15.05% (Arrhenius), 17.32% (strain compensated), 4.78% (Physical model) and 1.96% (ANN). The statistical analyses indicate that the trained ANN model exhibited the highest prediction accuracy for predicting the flow stress behaviour of the AISI 304 stainless steel.

Graphical Abstract

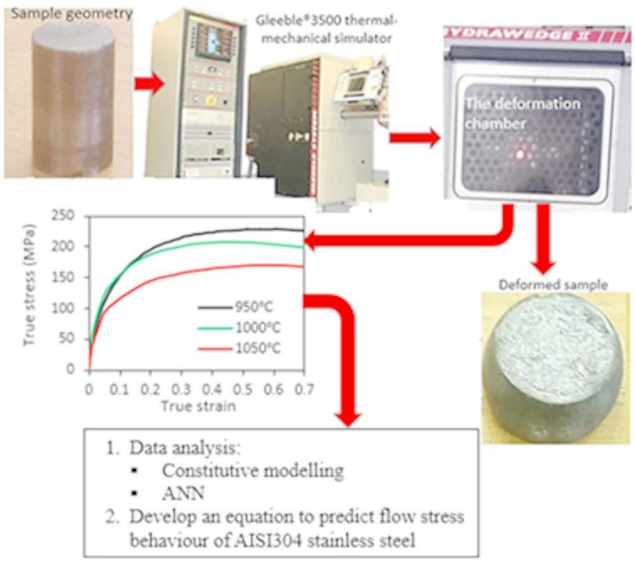

Keywords Flow stress behaviour · AISI 304 stainless steel · Constitutive model · ANN model · Statistical parameters

✉ Japheth Obiko
japheth.obiko97@gmail.com

[1] Department of Chemical, Metallurgical and Materials Engineering, Tshwane University of Technology, Pretoria, South Africa

Published online: 30 October 2025

1 Introduction

Metal forming processes are the most common industrial manufacturing techniques for machine components. Product quality during forming requires accurate and efficient analysis of metal flow patterns and optimisation of process parameters. Constitutive equations are widely used to study metal flow behaviour over the years [1–6]. These equations model the relationship between the flow stress and loading conditions such as temperature, strain and strain rate. The constitutive equations provide insights into the flow stress behaviour. Hence, these equations act as input codes for the computational modelling of metal forming [7–12]. The constitutive modelling equations, such as phenomenological/empirical (such as Arrhenius, JC model, Z-A model) and physical models (such as DRV/DRX model and Creep theory model), are classified based on the parameters involved in the quantitative analysis of the flow stress behaviour [13]. However, empirical models, such as Arrhenius equations, are widely used to analyse metal flow behaviour [3, 14, 15]. These models describe the relationship between flow stress and deformation conditions. Equation 1 describes the simplest empirical model as follows:

$$\dot{\varepsilon} = A f(\sigma) exp\left(\frac{-Q}{RT}\right) \tag{1}$$

where $\dot{\varepsilon}$ is the strain rate (s^{-1}), T is the temperature (K), Q is the activation energy of deformation (kJ.mol^{-1}), and R is the universal gas constant (8.314 Jmol^{-1} K^{-1}). The stress function $f(\sigma)$, which is the maximum flow stress value (peak stress σ_p) can be expressed as:

$$f(\sigma) = f(x) = \begin{cases} \sigma^{n'} & \alpha\ \sigma\ < 0.8 \\ \exp(\beta'\sigma) & \alpha\ \sigma\ > 1.2 \\ [\sinh(\alpha\sigma)]^n & for\ all\ flow\ stress \end{cases}$$

where n, n', β and α are material constants and $\alpha \approx \beta'/n'$.

Most studies have extensively used the sine law equation suggested by Sellars and Tergat [16], as in Eq. 2 for analysing hot workability of metals and alloys.

$$\dot{\varepsilon} = A[\sin h(\alpha\sigma)]^n \left[\frac{-Q}{RT}\right] \tag{2}$$

Equation 2 suggests that the hot deformation process is thermally activated. Therefore, the strain rate equation commonly used in creep analysis can describe the hot deformation process. Then, the flow stress behaviour analysis is by using the relationship between the Zener-Hollomon parameter (Z) and the flow stress as follows [17, 18]:

$$Z = \dot{\varepsilon} \exp\left(\frac{Q}{RT}\right) = f(\sigma) \tag{3}$$

In Eq. 3, f*(σ)* is similar as in Eq. 1. The hyperbolic sine law Eq. 2 is suitable for a wide range of loading conditions (temperatures and strain rates). The material constants in Eq. 2 (A, α, n and Q) depend on the chemical composition of the material. These material constants do not account for microstructure evolution during deformation. Hence, these parameters are referred to as apparent values [19, 20]. The material constants and activation energy Q obtained using the Arrhenius equation deviate from the theoretical values due to the influence caused by microstructural changes during deformation. Wang et al. [19] suggested that the normalisation flow stress by Young's Modulus $E(T)$ to account for the microstructure changes during deformation. Mirzadeh, Cabrera and Najafizadeh [21] proposed physically based equations to account for the self-diffusion of austenite and Young's Modulus temperature dependency as in Eq. 4:

$$\frac{\dot{\varepsilon}}{D(T)} = B[sinh(\alpha\sigma/E(T))]^n \tag{4}$$

$$D(T) = D_0 exp(-Q_{sd}/RT) \tag{5}$$

$$E(T) = E_0\left[1 - \frac{T_m}{G_0}\frac{dG}{dT}\frac{(T-300)}{T_m}\right] \tag{6}$$

The quantities in Eqs. 4–6 are defined, D_0 is the pre-exponential constant, Q_{sd} is the self-diffusion activation energy, $E(T)$ is Young's Modulus of the material at different deformation temperature, T_m is the material melting temperatures, $\dot{\varepsilon}$ is the strain rate (s^{-1}), B is the hyperbolic sine constant, α is the stress multiplier ($\alpha \approx \beta'/n'$), n is the stress exponent, E_0 is Young's modulus at temperature 300 K, $T_m/G_0.dG/dT$ is the temperature dependence of the modulus, G_0 is the shear modulus at 300 K, and D is the self-diffusion coefficient. The D_0,$E(T)$ and Q_{sd} values are obtained from Ashby Tables [22] for the deformation behaviour of materials.

Constitutive models are used to describe the metal flow behaviour of most metals and alloys during forming. These equations form the computer input codes for forging simulation. The simulation data depends on the efficient and accurate quantitative analysis of flow stress behaviour using the constitutive equations. However, material response during forming is nonlinear. Hence, the prediction accuracy of flow stress behaviour using these constitutive models is relatively low. Therefore, to address this challenge, Artificial Neural Networks (ANN) is an alternative approach for analysing metal forming. ANN has the capability of solving more complex nonlinear problems than the most constitutive models. This technique is a reliable approach to process

control and modelling of nonlinear problems. Several studies have used ANN to predict the flow stress behaviour of metals and alloys [23–28]. Study results show that ANN-predicted data has a good correlation with experimental data.

The quantitative techniques mentioned above form the basis of solving metal-forming processes. However, a question that remains unanswered is which of these models is well suited to analyse the metal flow behaviour of metals and alloys during deformation, especially AISI 304 stainless steel? This question requires an urgent answer to provide the basis for designing and scheduling metal-forming processes such as forging. However, a comprehensive, direct comparison of phenomenological, physically based, and machine learning models for predicting the hot workability of AISI 304 stainless steel under a wide range of industrial conditions has not been systematically performed. The current study carefully investigated the hot workability of AISI 304 stainless steel using constitutive models. The models include the Arrhenius model, the strain-compensation model, the physical model, and the Artificial Neural Networks model. Furthermore, the study compared the accuracy of these models in predicting the flow stress behaviour of the studied steel.

2 Experimental procedure

2.1 Uniaxial compression test

After production, most structural and functional components undergo a metal-forming process to improve their mechanical properties. To study the metal flow pattern, Gleeble® thermal-mechanical equipment assists in testing metal flow behaviour under a controlled environment. In this study, the test samples used were standard AISI 304 stainless steel measuring 8 mm in diameter and 15 mm in length. Uniaxial compression test conditions were 950, 1000 and 1050 °C, and strain rates of 0.1, 1, 10 and 15 s^{-1}. The K-type thermocouples welded at the mid-length of the sample monitor the test temperature against the preset temperature during testing. For reduced interfacial friction between the specimen and the ISO-T anvils, this study used nickel pastes and graphite foil. The deformation process involves heating the specimens to an austenitisation temperature of 1100 °C at a heating rate of 5 °C/s and holding them at this temperature for 180 s. Then, the specimens undergo a 10 °C/s cooling rate to the deformation temperature. Before deformation, the test sample is soaked for 60 s to reduce the thermal gradient. Deformation was up to 0.7 true strain and then air-cooled rapidly to room temperature. The deformation temperature used for typical forging ensures that the material undergoes forging in the single-phase austenite for steel. This deformation temperature ensures good workability [29]. The computer control system converts load and displacement data to flow stress-strain data. The analysis of this data using a constitutive model develops a constitutive model that can predict the flow stress behaviour of the material studied under the investigated loading conditions.

2.2 Artificial neural network ANN

This study utilised the flow stress-strain data for Artificial Neural Network (ANN) analysis. Figure 1 illustrates the ANN architecture used in this study, built using the MATLAB platform. The network has two hidden layers, the first layer uses the hyperbolic sigmoid transfer function "tansig", while the second layer uses the pure linear transfer function "purelin". The temperature, strain rate and strain were the inputs while the flow stress was the output. In ANN modelling, the range of input and output data should range between 0 and 1. Therefore, the input and output data were normalised before use in the network. The strain rate, temperature (T^{-1} in K^{-1}), and strain (ε) are the input factors used to predict the normalised output, $\sigma/\sigma max$. The strain rate variation this study was very high. Therefore, Eq. 7 was used to normalise the strain rate. The normalisation assists in preventing variation during ANN model training [30].

$$\dot{\varepsilon}' = 0.1 + 0.8 \times \left(\frac{\ln \dot{\varepsilon} - \ln \dot{\varepsilon}_{\min}}{\ln \dot{\varepsilon}_{\max} - \ln \dot{\varepsilon}_{\min}} \right) \tag{7}$$

Where $\dot{\varepsilon}'$ is the normalised strain rate, $\dot{\varepsilon}_{\max}$ is the maximum strain rate and $\dot{\varepsilon}_{\min}$ is the minimum strain rate. The ANN model utilises derived flow stress-strain data as follows: 70% for training, while validation and testing of the ANN model uses 15% of the data. The input and output data should have a balanced neuron activation and weight distribution. The same data range will enhance training speed and accuracy. Table 1 shows the experimental data and the normalised inputs and output ANN model data. The appropriate number of hidden layers were determined using trial and error. The hidden layer consists of 10 hidden neurons. Generally, the model uses the Levenberg-Marquardt back-propagation training algorithm to train the network. This algorithm provides an effective means of analysing nonlinear least-squares problems [24, 25]. Table 2 shows the chemical composition of the steel studied.

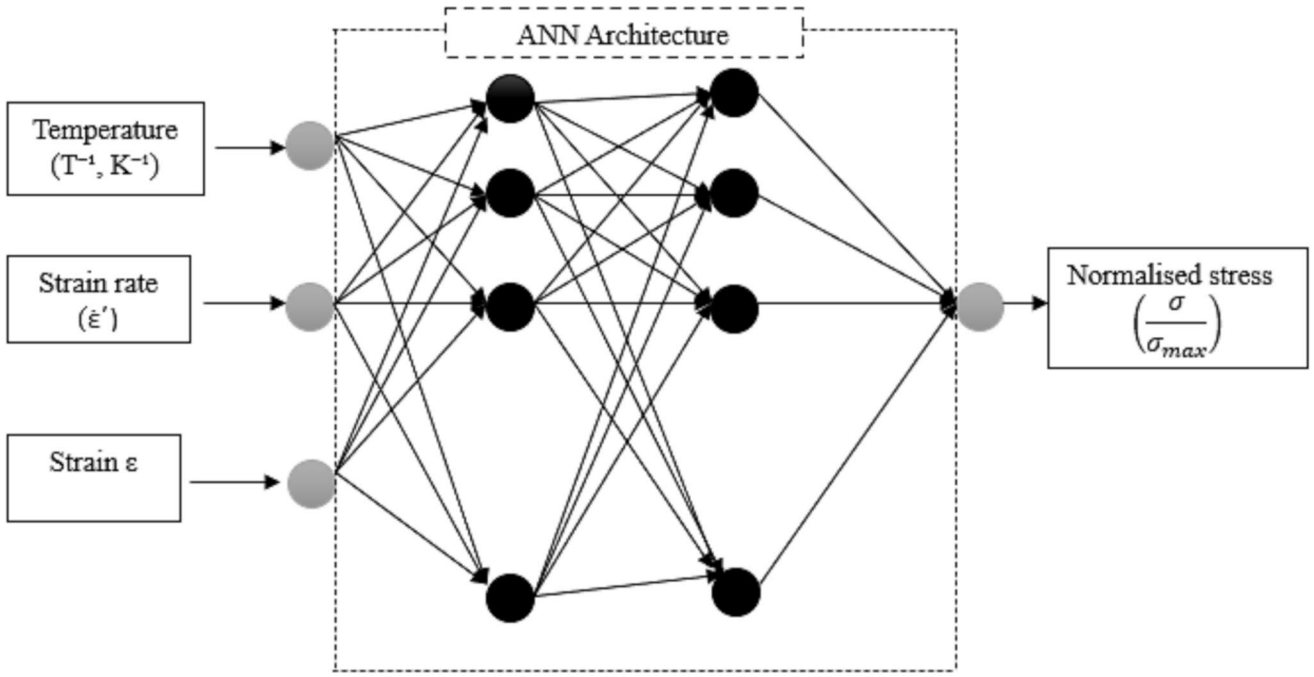

Fig. 1 ANN architecture in this study

Table 1 Experimental and ANN model values

	Experimental values	Input/output for ANN model
Temperature	950, 1000, 1050 °C	$\frac{1}{T}$, $[7.56\times10^{-4} - 8.18\times10^{-4}]$ K^{-1}
Strain rate	0.1, 1, 10, 15 s^{-1}	$\dot{\varepsilon}'$ [0.1–0.9]
Strain	0.1, 0.2, 0.3, 0.4, 0.5, 0.6, 0.7	ε, [0.1–0.7]
Stress	[40.27– 228.56] MPa	$\frac{\sigma}{\sigma_{\max}}$, [0.176–1]

Table 2 Chemical composition of AISI 304 stainless steel studied

C	Mn	Si	*P*	Cr	Ni	*N*	S
0.01	1.43	0.34	0.01	18.4	8.30	0.05	0.002

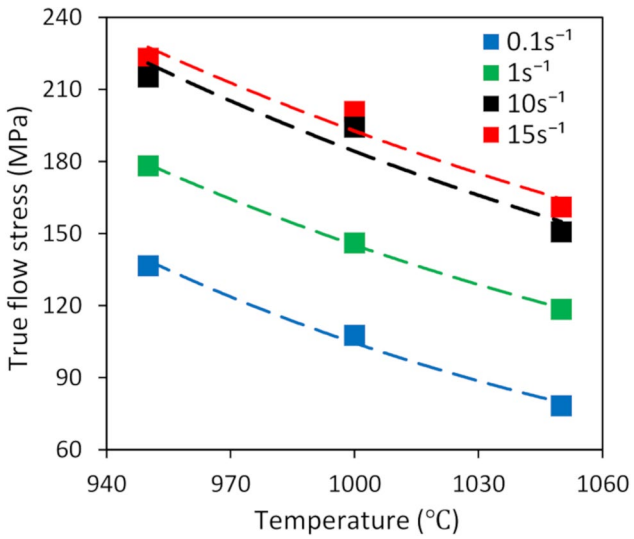

Fig. 2 A plot of true flow stress vs. deformation temperature

3 Results and discusssion

3.1 Flow stress behaviour

Figure 2 shows the plot of flow stress data at different loading conditions (deformation temperature and strain rate) derived from the flow stress-strain curves. The results show an increase in flow stress with a decrease in deformation temperature and an increase in strain rate and vice versa. This phenomenon is due to the change in the deformation mechanism. At higher temperatures, a dynamic softening is more pronounced, resulting in a lower flow stress. This behaviour is due to an increase in atom diffusion rate and dislocation movement [31]. However, low deformation temperatures and high strain rates result in the high generation of dislocation density, causing work hardening behaviour. Hence, higher flow stress. From the plots, therefore, results show that the metallurgical behaviour of the flow

stress pattern indicates that the flow stress is sensitive to the deformation temperature and strain rate. However, further details on the characteristic behaviour of flow stress-strain curves and microstructure characterisation will be discussed elsewhere by the present authors. In this study, therefore, the research focussed on an investigation of the material behaviour at different loading conditions using constitutive and ANN models. Table 3 shows the flow stress values at different deformation temperatures and strain rates used in this analysis.

3.2 Arrhenius constitutive analysis

The Arrhenius equations were used in this study to describe the effect of loading conditions on the flow stress behaviour of AISI 304 stainless steel. The material constants and activation energy in the constitutive equations during deformation are obtained using the peak stress σp or the steady-state stress [32]. However, some material did not exhibit a clear peak stress or a steady-state region after the peak. Therefore, the material constants and the activation energy were determined using the saturation flow stress σss [33], which occurs when an increase in the flow stress is limited by dynamic recovery, hence reaching a steady-state value. These flow stress values can be obtained directly from the flow stress-strain curve and applied in modelling the flow stress behaviour over a wide range of deformation conditions [34, 35]. Therefore, in this study, the analysis used saturation flow stress. From Eq. 1, the material constants n' and β' can be determined using the power law and exponential law equations for high and low flow stress and $\alpha \approx \beta'/n'$. Therefore, taking natural logarithm into Eq. 1 gives:

$$\text{Low stress} : \dot{\varepsilon} = A_1 {\sigma_{ss}}^{n'} \exp\left(\frac{-Q}{RT}\right) \tag{8}$$

$$\text{High stress} : \dot{\varepsilon} = A_2 \exp\left(\beta\sigma_{ss}\right) \exp\left(\frac{-Q}{RT}\right) \tag{9}$$

Taking the natural logarithms of the equations:

$$\ln\dot{\varepsilon} + \frac{Q}{RT} = \ln A_1 + n' \ln\sigma_{ss} \tag{10}$$

$$\ln\dot{\varepsilon} + \frac{Q}{RT} = \ln A_2 + \beta\sigma_{ss} \tag{11}$$

Table 3 Flow stress value for AISI 304 stainless steel

Factors	950°C	1000°C	1050°C
$0.1s^{-1}$	136.74	107.76	78.42
$1s^{-1}$	178.31	146.23	118.61
$10s^{-1}$	215.25	194.40	150.82
$15s^{-1}$	223.13	200.81	161.04

Taking the partial derivatives of Eqs. 10 and 11 at constant deformation temperature, gives:

$$n' = \frac{\partial \ln\dot{\varepsilon}}{\partial \ln\sigma_{ss}} \tag{12}$$

$$\beta' = \frac{\partial \ln\dot{\varepsilon}}{\partial\sigma_{ss}} \tag{13}$$

Solving Eqs. 12 and 13 gives a linear relationship between the two variables. The β' values determined from the slope of $\ln\dot{\varepsilon}$ *vs.* σ_{ss} plots (Fig. 3a) and n' value is obtained by taking average slope of $\ln\dot{\varepsilon}$ *vs.* $\ln\sigma_{ss}$, (Fig. 3b). Then, solving the universal hyperbolic sine function (Eq. 2), at a constant temperature and taking the natural logarithm to both sides of the equation and partial derivative with$\ln\dot{\varepsilon}$ gives Eq. 14:

$$\frac{1}{n} = \frac{\partial \ln\left[\sinh\left(\alpha\sigma_{ss}\right)\right]}{\partial \ln\dot{\varepsilon}} \tag{14}$$

Similarly, at constant strain rate $\dot{\varepsilon}$ give Eq. 15:

$$Q = Rn\frac{\partial \ln\left[\sinh\left(\alpha\sigma_{ss}\right)\right]}{\partial\frac{1}{T}} \tag{15}$$

Therefore, the stress exponent n-value is obtained by taking the average of the slope of the plots of $\ln\dot{\varepsilon}$ vs. ln sinh ($\alpha\,\sigma_{ss}$) at different deformation temperatures (Fig. 4a). The activation energy Q is determined from the plot of ln sinh ($\alpha\,\sigma_{ss}$) vs. $1000/T$ at different strain rates (Fig. 4b).

The effect of deformation temperature and strain rate on the flow stress (σ) can be well described using Zener-Hollomon parameter (Z) [17, 18], and the relationship between Z and σ is expressed in Eq. 16:

$$Z = \dot{\varepsilon}\exp\left[\frac{Q}{RT}\right] = A[\sinh\left(\alpha\sigma_{ss}\right)]^n \tag{16}$$

Taking the natural logarithm to Eq. 16, gives Eq. 17. A plot of *sinh* ($\alpha\sigma_{ss}$) *vs. ln Z* (Fig. 5) gives material constants A and n values.

$$\ln Z = \ln A + n\sin h\left(\alpha\sigma_{ss}\right) \tag{17}$$

Solving Eq. 16, the flow stress σ_{ss} can be calculated using Eq. 18:

$$\sigma_{ss} = \frac{1}{\alpha}\ln\left\{\left(\frac{Z}{A}\right)^{1/n} + \left[\left(\frac{Z}{A}\right)^{2/n} + 1\right]^{1/2}\right\} \tag{18}$$

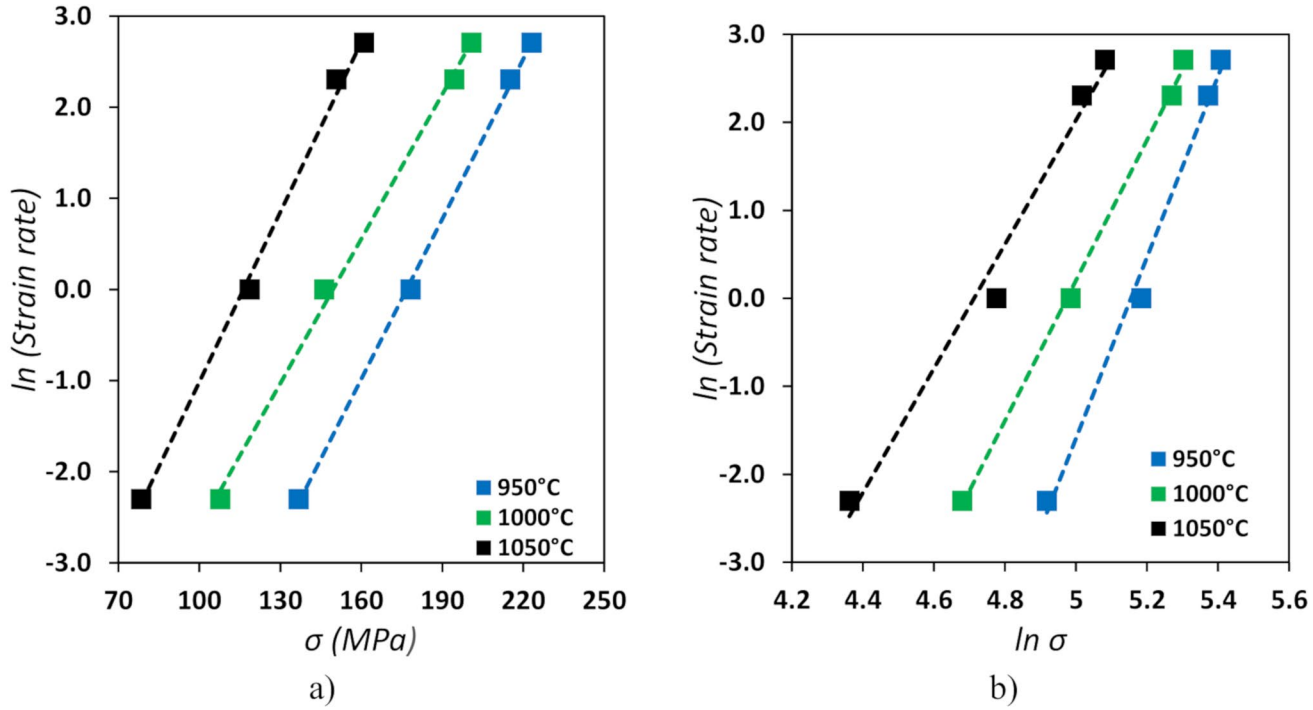

Fig. 3 Graph of (**a**) *ln* ($\dot{\varepsilon}$) vs. σ to obtain β, and (**b**) *ln* ($\dot{\varepsilon}$) *vs. ln* σ to obtain *n′*

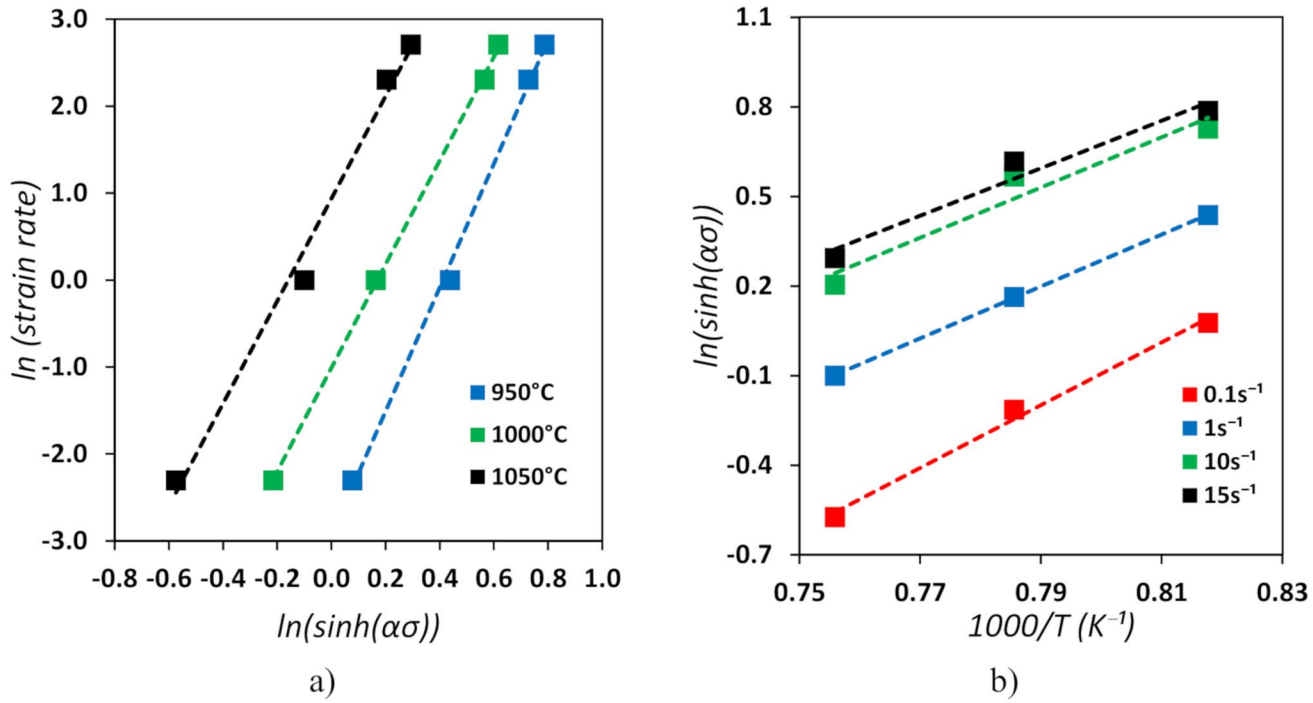

Fig. 4 Plot of (**a**) *ln* ($\dot{\varepsilon}$) vs. ln (sinh ($\alpha\sigma_{sat}$) to determine stress exponent *n*, and (**b**) *ln* (sinh ($\alpha\sigma_{sat}$)) vs. 1000/T to obtain activation energy *Q*

The material constants calculated using the constitutive equations for the studied steel were $n'=8.44$, and $\beta'=0.0578$. Therefore, the stress multiplier $\alpha \approx \beta'/n'=0.00685$. The calculated stress exponent $n=6.32$, which is relatively consistent with the conventional values reported in the literature [36]. The Q-value was 467.40 kJ.mol-1, and the shape factor $A=1.865 \times 1.865 \times 10^{18}$ (Fig. 5). The obtained *Q*-value for this steel lies within the range of 360 ~ 475

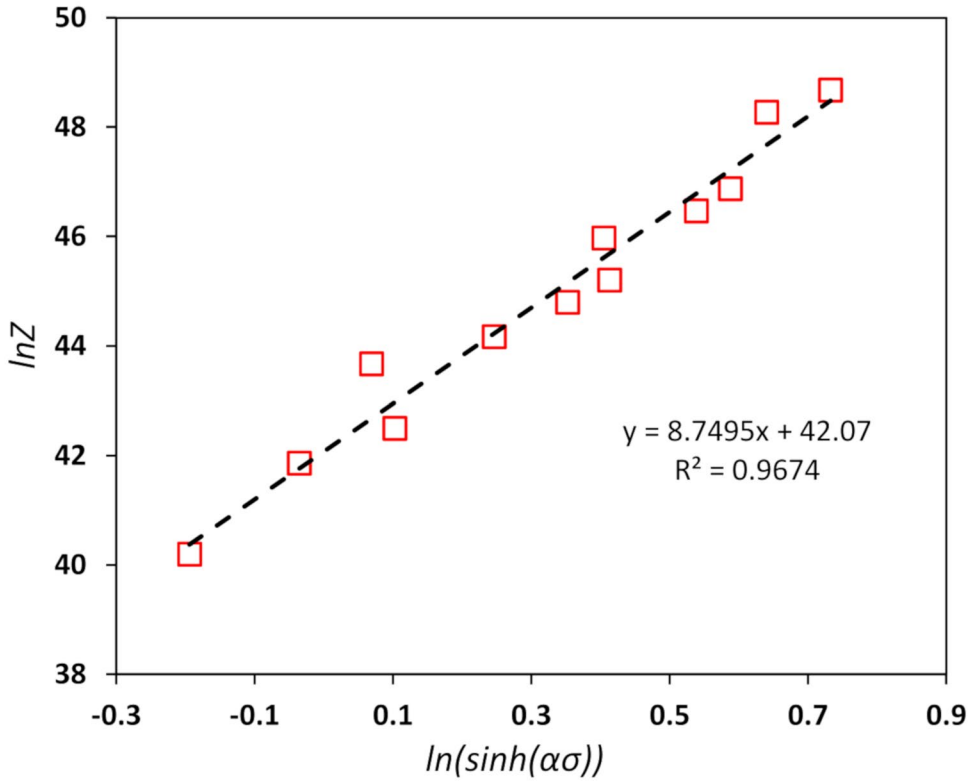

Fig. 5 A comparison between *ln Z* and *ln* (sinh ($\alpha\sigma_{ss}$)) at all forming conditions

kJmol^{-1} reported in the literature [36–38]. These material constants and activation energy are substituted in Eq. 2 to develop the constitutive equation that can predict the flow stress behaviour of the steel studied:

$$\dot{\varepsilon} = 1.865 \times 10^{18} \sin h(0.00685\sigma_{sat})^{6.32} exp\left[\frac{-467400}{RT}\right] \tag{19}$$

The flow stress for AISI 304 stainless steel:

$$\sigma_{ss} = \frac{1}{0.00685} \ln\left[\left(\frac{Z}{1.865 \times 10^{18}}\right)^{\frac{1}{6.32}} + \left(\left(\frac{Z}{1.865 \times 10^{18}}\right)^{\frac{2}{6.32}} + 1\right)^{\frac{1}{2}}\right] \tag{20}$$

$$Z = \dot{\varepsilon}\left[\frac{467400}{RT}\right] = 1.865 \times 10^{18}(\sin h\,(0.00685\sigma_{ss}))^{6.32} \tag{21}$$

3.3 Strain compensation arrhenius analysis

Studies show that strain affects the flow stress behaviour during forming [39, 40]. Therefore, the accuracy of the flow stress requires an account of the effect of the strain. The material constants (α *n*, *Q*, *lnA*) calculated in Sect. 3.2 are strain-dependent for the entire strain range. These material constants are assumed to be polynomial functions of strain. To this end, therefore, these material constants should be determined at each strain level. In this study, the calculated material constants were at the strain range of 0.1–0.7 at an interval of 0.1. Fitting the material constants against strain plots gives polynomial functions form, as shown in Eq. 22:

$$\begin{aligned} \alpha &= A_0 + A_1\varepsilon + A_2\varepsilon^2 + A_3\varepsilon^3 + \cdots + A_n\varepsilon^n \\ n &= B_0 + B_1\varepsilon + B_2\varepsilon^2 + B_3\varepsilon^3 + \cdots + B_n\varepsilon^n \\ \mathrm{Q} &= \mathrm{C}_0 + \mathrm{C}_1\varepsilon + \mathrm{C}_2\varepsilon^2 + \mathrm{C}_3\varepsilon^3 + \cdots + \mathrm{C}_n\varepsilon^n \\ \ln A &= D_0 + D_1\varepsilon + D_2\varepsilon^2 + D_3\varepsilon^3 + \cdots + D_n\varepsilon^n \end{aligned} \tag{22}$$

Table 4 Polynomial coefficients for strain compensation

ε	α	*n*	Q	lnA
0.1	0.0108	5.45	538.85	48.72
0.2	0.00789	5.584	392.01	35.054
0.3	0.00702	5.922	378.04	33.755
0.4	0.00672	6.094	371.17	33.115
0.5	0.00654	5.73	325.46	28.862
0.6	0.00674	5.62	369.2	32.932
0.7	0.00659	6.72	496.61	44.788

The optimal polynomial order is determined by varying polynomial order *n* from one to nine to obtain a good correlation and generalisation. The constitutive model is derived from the calculated material constants. Table 4

shows the polynomial coefficients after the 6th polynomial order obtained using the constitutive equations discussed in Sect. 3.2. Figure 6 shows data plots of material constants versus the strain. The results show variation in material constant values as affected by the deformation degree (strain). This variation may be due to changes in the microstructure evolution during forming. These microstructure changes indicate the mechanism occurring during the forming process. The deformation mechanisms influence product quality. Hence, product response to mechanical properties.

3.4 Physically-based modelling

The material constants obtained in Sect. 3.2 and 3.3 using Arrhenius equations do not account for microstructure changes during deformation. Hence, researchers refer to these values as apparent values [19]. These constants deviate from the theoretical values. The reason is that the microstructure change influences the deformation process. According to Wang et al. [19], the variation can be reduced by flow stress normalisation using Young's Modulus $E\,(T)$, which varies with deformation temperature. Therefore, Eq. 4 addresses this concern. This study analysed the flow stress behaviour using physically-based Eqs. 4–6.

The power and exponential law equation can be written as:

$$\text{For low stresses}: \frac{\dot{\varepsilon}}{D\,(T)} = B_1\left(\frac{\sigma_{ss}}{E\,(T)}\right)^{n\prime} \tag{23}$$

$$\text{For high stresses}: \frac{\dot{\varepsilon}}{D\,(T)} = B_2 \exp\left(\frac{\beta\prime\sigma_{ss}}{E\,(T)}\right) \tag{24}$$

Equations 23 and 24 were used to determine the material constants $n\prime$ and $\beta\prime$ in all tested deformation conditions. The $\beta\prime$-value was obtained by taking the slope of the plot $\ln\dot{\varepsilon}/D\,(T) - (\sigma_{ss}/E\,(T))$ (Fig. 7a). The $n\prime$ value is the slope of the plot $\ln\dot{\varepsilon}/D\,(T) - \ln\,(\sigma_{ss}/E\,(T))$ (Fig. 7b). The obtained values were: $\beta\prime$=6288.4, $n\prime$=7.6352 and $\alpha \approx \beta\prime/n\prime$=823.61. The stress exponent n (gradient) and ln B (intercept) values were from a plot of $\ln\dot{\varepsilon}/D\,(T) - \ln(\sinh(\alpha\sigma_{sat}/E\,(T)))$, as in Fig. 7c). The linear regression analysis of the plot gives, stress exponent n=5.79 and ln B=35.703. Table 5 gives a summary of the calculated material constant α, B and n values for different deformation conditions. Substituting the material constants in Eq. 4 gives Eq. 25. This developed a constitutive equation that can predict the flow stress for the studied steel:

$$\dot{\varepsilon}\exp\left[\frac{280000}{RT}\right] = 1.185\times10^{11} \left[\sin h\,(823.61\times\sigma_{ss}/E\,(T))\right]^{5.79} \tag{25}$$

Using hyperbolic sine function properties, Eq. 4 becomes:

$$\left(\frac{Z}{B}\right)^{\frac{1}{n}} = \sin h\left(\alpha\frac{\sigma_{sat}}{E\,(T)}\right) = \frac{e^{\alpha\sigma_{sat}/E(T)}}{2} - \frac{-e^{\alpha\sigma_{sat}/E(T)}}{2} \tag{26}$$

Solving Eq. 26 gives Eq. 27:

$$\sigma_{sat} = \frac{E\,(T)}{\alpha} \ln\left[\left(\frac{Z}{B}\right)^{\frac{1}{n}} + \left(\left(\frac{Z}{B}\right)^{\frac{2}{n}} + 1\right)^{\frac{1}{2}}\right] \tag{27}$$

Equation 27 can be used to determine the flow stress values at different loading conditions. Therefore, the equation for predicting the flow stress for AISI 304 stainless steel studied under different deformation conditions, is as in Eq. 28 and $Z = \dot{\varepsilon}\exp\left(\frac{33678.13}{T}\right)$:

$$\sigma_{sat} = \frac{E\,(T)}{823.61} \ln\left[\left(\frac{Z}{1.185\times10^{11}}\right)^{\frac{1}{5.79}} + \left(\left(\frac{Z}{1.185\times10^{11}}\right)^{\frac{2}{5.79}} + 1\right)^{\frac{1}{2}}\right] \tag{28}$$

3.5 Artificial neural network evaluation

Machine learning tools such as ANN have become the most superior tools for solving complex non-linear problems without using the widely used constitutive equations. ANN models can optimise process parameters, such as forging process parameters, to determine the optimal input factors. This technique learns and reorganises data using discrete data sets. The computational procedure for ANN is readily available in the literature [25, 28, 30]. Hence, there is no need to duplicate the same information in this article. Readers can get information on the ANN computational procedure and analysis in the literature. In this study, therefore, the application of ANN to analyse the metal forming process followed the procedure and ANN architecture as per Jenab et al. [24]. Figure 8 shows the performance of the developed ANN model in this study. The results indicate a good correlation between the predicted and experimental data over a wide range of loading conditions. From these results, the study observed that ANN has high prediction accuracy for the flow stress behaviour of AISI 304 stainless steel at different loading conditions. Generally, the results indicate that the trained ANN model can effectively predict the flow stress behaviour of the studied steel.

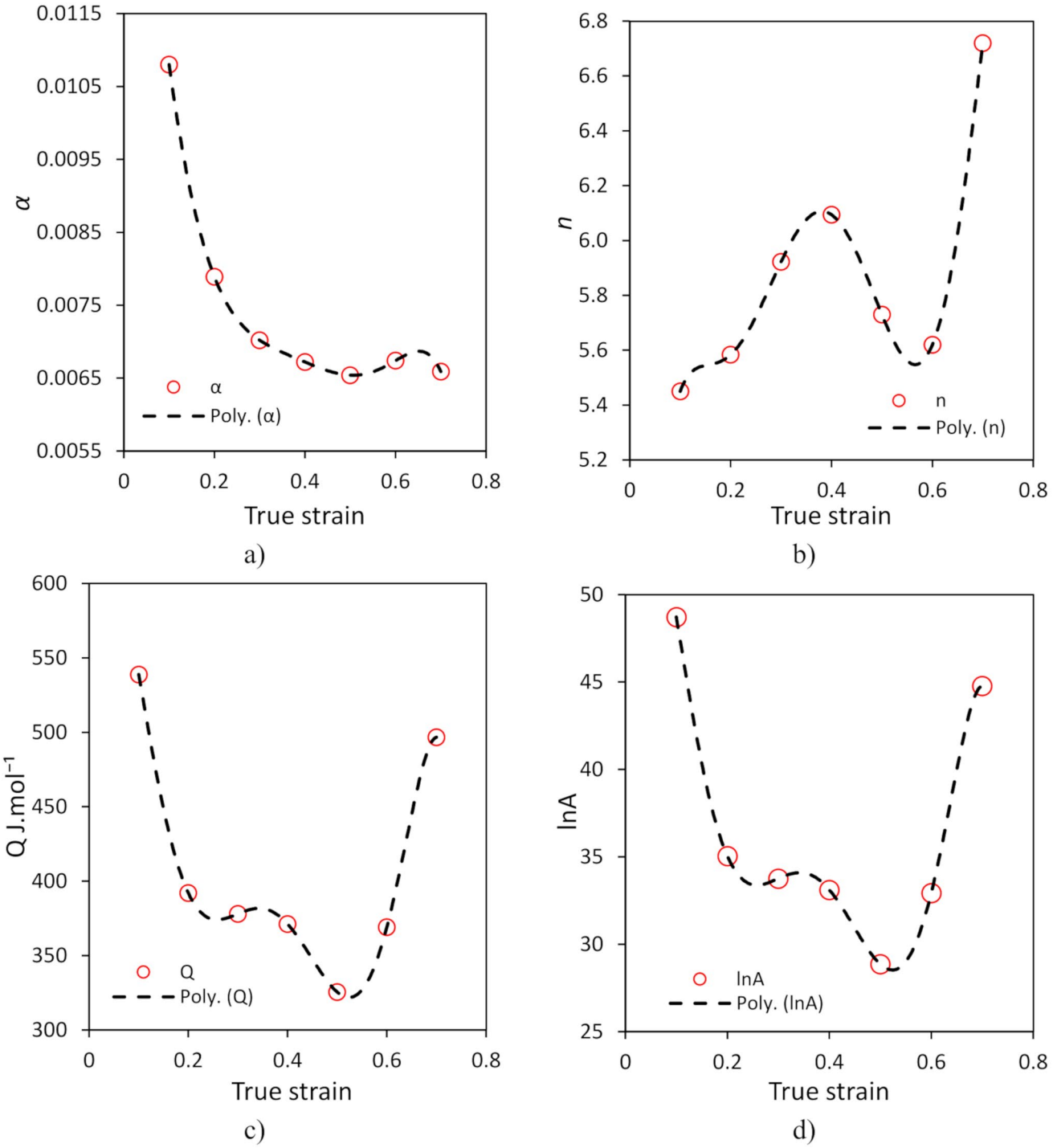

Fig. 6 Variation of (**a**) α (**b**) n (**c**) Q (**d**) lnA vs. true strain

ANN tools have a wide application in studying the metal flow of various metals and alloys [24, 28, 30]. Studies have shown that ANN has high accuracy in predicting the flow stress compared to other constitutive models. For example, Xiao et al. [28] studied the flow behaviour of 12Cr3WV steel using constitutive and ANN models. The study findings show that ANN has a better capability in predicting flow stress behaviour compared to the strain-compensated model. Similar results have been reported in the literature, indicating that ANN has high prediction accuracy compared to constitutive Eqs [24, 25, 30, 41]. Therefore, the ANN model is capable of completely describing the flow behaviour. The model can develop a generic constitutive model to predict the flow behaviour of any alloy. However, the

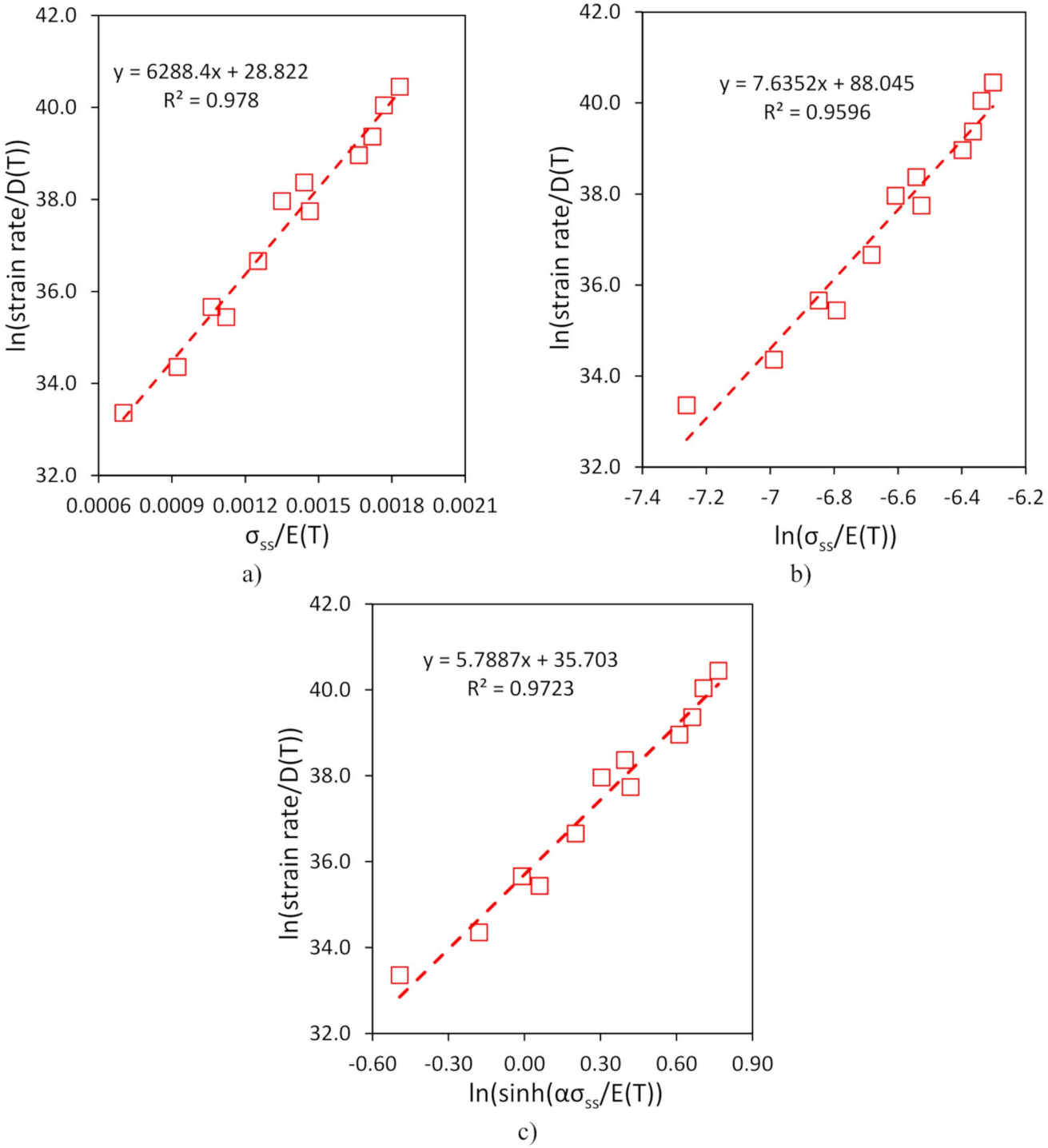

Fig. 7 Plots for determining material constants: (**a**) β, (**b**) n' and (**c**) n using the physical based model

Table 5 Calculated material constants for warm deformation

Material constants	α	n	B
Value	823.61	5.79	1.185×10^{11}

ANN constitutive model requires a large amount of data. The availability of these data depends on the complexity of the metal flow pattern. Sometimes these data may not be available. Hence, a lack of data reduces the accuracy of the model in predicting flow behaviour.

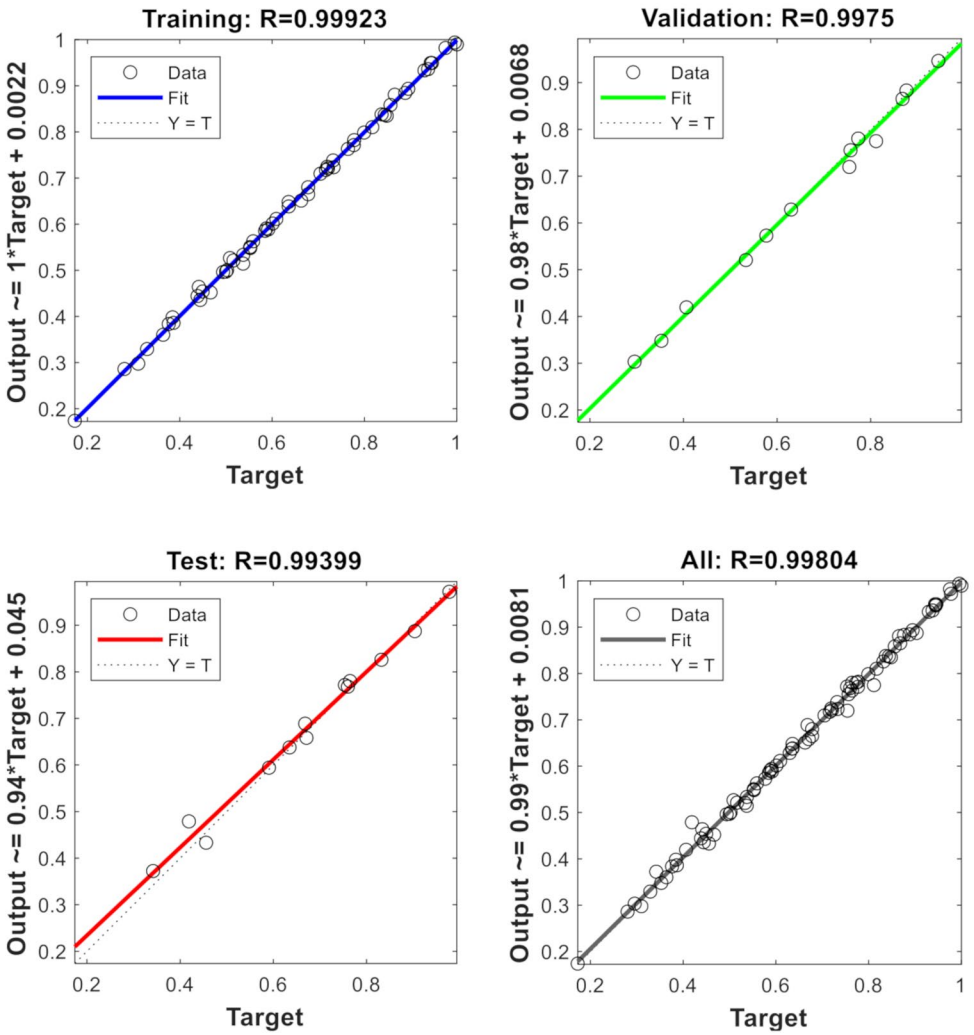

Fig. 8 Plots showing the performance of the ANN model

4 Models validation

A comparison between the predicted flow stress and experimental flow stress at different loading conditions can be analysed and reported, as shown in Fig. 9. The comparison was done using statistical parameters: Pearson's correlation coefficient R (using Eq. 29) and the average absolute relative error $AARE$ (using Eq. 30). These parameters check the accuracy of the constitutive and ANN models in predicting the flow stress of the studied steel. These parameters (R and $AARE$) show the linear relationship between two variables. This statistical approach validates the developed constitutive model to predict flow stress [14, 42, 43].

$$R = \frac{\sum_{i=1}^{N}\left(Y_i - \bar{Y}\right)\left(X_i - \bar{X}\right)}{\sqrt{\sum_{i=1}^{N}\left(Y_i - \bar{Y}\right)^2 \sum_{i=1}^{N}\left(X_i - \bar{X}\right)^2}} \tag{29}$$

$$AARE\,(\%) = \frac{1}{N}\sum_{i=1}^{N}\left[\frac{Y_i - X_i}{Y_i}\right] \tag{30}$$

where Y is the measured flow stress, X is the predicted saturation flow stress and, $\bar{Y}$ is the average values of Y and $\bar{X}$ is the average values X. The N term is the total data points used in the analysis. Figure 9 shows the scatter plot of the experimental and predicted flow stress. From the plots, the Pearson's correlation coefficient for the three models were 0.994 (Arrhenius), 0.994 (strain compensated), 0.980 (Physical model) and 0.998 (ANN). The results show that the predicted and experimental flow stress exhibited a good correlation. According to [13], Pearson's correlation coefficient results may be biased towards higher or lower values. Hence, may give an invalid relationship between the compared variables. Therefore, the AARE analysis provides more accurate results. Thus, it is a good parameter for statistical analysis. This parameter generally gives the accuracy of the model by determining the relative error for each term of the flow stress. The obtained percentage relative error for the three models were 15.05% (Arrhenius), 17.32% (strain compensation), 4.78% (Physical model) and 1.96% (ANN). On the other hand, the coefficient of determination

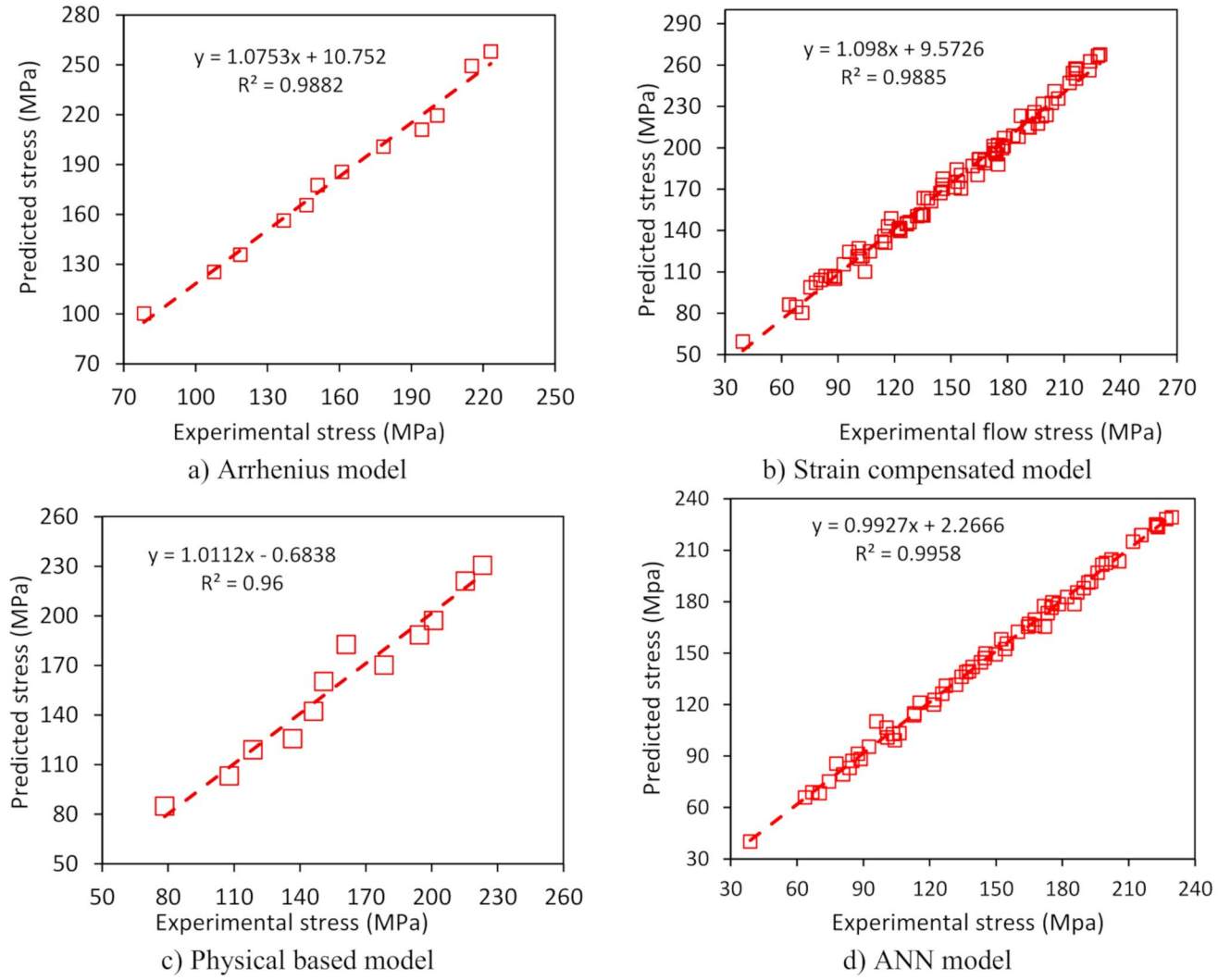

Fig. 9 Figure 9. A comparison between the predicted and experimental flow stress using different models

was 0.9882 (Arrhenius), 0.9885 (strain compensated), 0.960 (Physical model) and 0.9958 (ANN). The results of the statistical models show that all the developed models exhibited good accuracy in predicting the flow stress for the studied steel. However, ANN gave the best prediction model for the flow stress behaviour. The study findings indicate that the application of ANN in metal forming will provide a paradigm shift in metal flow behaviour analyses. This technique assists in optimising process parameters, predicting material properties and improving process control. Hence, improving product quality. Generally, ANN tools have enhanced the prediction of output variables given a new set of inputs, thus improving design, simulation and solving real-world physical problems in manufacturing.

5 Conclusion

In this study, the flow stress-strain data was obtained from uniaxial compression tests using the Gleeble® thermal-mechanical equipment at a temperature range of 950–1050°C and strain rate of 0.1–15 s^{-1}. These data assisted in the analysis of the metal flow behaviour of AISI 304 stainless steel using Arrhenius, strain compensation, physical-based and ANN models. From the results, the following were the conclusions:

1. The flow stress increased with a decrease in the deformation temperature and an increase in strain rate and vice versa. The results indicate that the flow stress is sensitive to the deformation conditions.
2. The statistical parameters R and AARE validated the models. The R-values were 0.994 (Arrhenius), 0.994 (strain compensated), 0.980 (Physical model) and 0.998

(ANN), and the AARE-values were 15.05% (Arrhenius), 17.32% (strain compensated), 4.78% (Physical model) and 1.96% (ANN).

3. For the four models, ANN had the highest prediction accuracy for predicting the flow stress behaviour of the AISI 304 stainless steel studied.
4. This study found that to improve industrial forming processes, the ANN model should be used to predict the flow pattern and optimise the process/input parameters (temperature, strain and strain rate) for high-quality products. Hence, reducing production cost and time.

Data availability The data used to support the findings of this study are included within the article.

Declarations

Conflict of interest The authors declare that they have no conflicts of interest regarding the publication.

References

1. Bodunrin, M., Obiko, J., Klenam, D.: On the uniaxial compression testing of metallic alloys at high strain rates: An assessment of DEFORM-3D simulation. Appl. Sci. **13**, 2686 (2023)
2. Kumar, N., Kumar, S., Rajput, S.K., Nath, S.K.: Modelling of flow stress and prediction of workability by processing map for hot compression of 43CrNi steel. ISIJ Int. **57**(3), 497–505 (2017). https://doi.org/10.2355/isijinternational.ISIJINT-2016-306
3. Yan, P., dong Liu, Z., Liu, W., Bao, H., Weng, Y.: Hot deformation behavior of a new 9%Cr heat resistant steel G115. J. Iron Steel Res. Int. **20**(9), 73–79 (2013). https://doi.org/10.1016/S1006-706X(13)60159-4
4. Obiko, J., Chown, L., Whitefield, D., Bodunrin, M.: Understanding hot workability of power plant P92 creep resistant steels using dynamic material modelling (DMM) and microstructural evolution. Int. J. Interact. Des. Manuf. (2022). https://doi.org/10.1007/s12008-022-01084-9
5. Maube, S., Obiko, J., Van Der Merwe, J., Mwema, F., Klenam, D., Bodunrin, M.: Comparative study on hot metal flow behaviour of Virgin and rejuvenated heat treatment creep exhausted P91 steel. Appl. Sci., (2023)
6. Sun, S.L., Zhang, M.G., He, W.W.: Hot deformation behavior and hot processing map of P92 steel. Advanced Mater. Research. 290–295 (2010). https://doi.org/10.4028/www.scientific.net/AMR.97-101.290
7. Zhu, L.: A two-stage constitutive model of X12CrMoWVNbN10-1-1 steel during elevated temperature. Mater. Res. Express. **5**, 1–11 (2018)
8. Wang, S., Huang, Y., Xiao, Z., Liu, Y., Liu, H.: A modified Johnson-cook model for hot deformation behavior of 35CrMo steel. Met. (Basel). **7**(9), 337 (2017). https://doi.org/10.3390/met7090337
9. Samantaray, D., Mandal, S., Bhaduri, A.K.: Constitutive analysis to predict high-temperature flow stress in modified 9Cr-1Mo (P91) steel. Mater. Des. **31**(2), 981–984 (2010). https://doi.org/10.1016/j.matdes.2009.08.012
10. Lin, Y.C., Chen, M.S., Zhang, J.: Modeling of flow stress of 42CrMo steel under hot compression. Mater. Sci. Eng. A. **499**, 1–2 (2009). https://doi.org/10.1016/j.msea.2007.11.119
11. Yin, F., Hua, L., Mao, H., Han, X.: Constitutive modeling for flow behavior of GCr15 steel under hot compression experiments. Mater. Des. **43**, 393–401 (2013). https://doi.org/10.1016/j.matdes.2012.07.009
12. Lin, Y.C., Chen, X.M.: A critical review of experimental results and constitutive descriptions for metals and alloys in hot working. Mater. Des. **32**, 1733–1759 (2011). no. 410.1016/j.matdes.2010.11.048
13. He, A., Xie, G., Yang, X., Wang, X., Zhang, H.: A physically-based constitutive model for a nitrogen alloyed ultralow carbon stainless steel. Comput. Mater. Sci. **98**, 64–69 (2015). https://doi.org/10.1016/j.commatsci.2014.10.044
14. Sun, C., Zuo, X., Xiang, Y., Yang, J.: Investigation on hot deformation behavior and hot processing map of BSTMUF601 Super-Alloy. Met. (Basel). **6**(3), 70 (2016). https://doi.org/10.3390/met6030070
15. Yang, H., Li, Z.H., Zhang, Z.L.: Investigation on Zener-Hollomon parameter in the warm-hot deformation behavior of CF53. J. Shanghai Jiaotong Univ. **12 E**, 352–358 (2007). https://doi.org/10.1631/jzus.2006.A1453
16. Sellars, C.M., McTegart, W.J.: On the mechanism of hot deformation. Acta Metall. **14**, 1136–1138 (1966). no. 910.1016/0001-6160(66)90207-0
17. Alsagabi, S.: High temperature deformation behavior of P92 steel. Trans. Indian Inst. Met. **69**(8), 1513–1518 (2016). https://doi.org/10.1007/s12666-015-0725-3
18. Wang, B., Fu, W., Lv, Z., Jiang, P., Zhang, W., Tian, Y.: Study on hot deformation behavior of 12%Cr ultra-super-critical rotor steel. Mater. Sci. Eng. A. **487**, 1–2 (2008). https://doi.org/10.1016/j.msea.2007.10.007
19. Wang, L., Liu, F., Cheng, J.J., Zuo, Q., Chen, C.F.: Hot deformation characteristics and processing map analysis for Nickel-based corrosion resistant alloy. J. Alloys Compd. **623**, 69–78 (2015). https://doi.org/10.1016/j.jallcom.2014.10.034
20. Mirzadeh, H., Cabrera, J.M., Najafizadeh, A.: Constitutive relationships for hot deformation of austenite. Acta Mater. **59**(16), 6441–6448 (2011). https://doi.org/10.1016/j.actamat.2011.07.008
21. Mirzadeh, H.: Simple physically-based constitutive equations for hot deformation of 2024 and 7075 aluminum alloys. Trans. Nonferrous Met. Soc. China (English Ed. **25**(5), 1614–1618 (2015). https://doi.org/10.1016/S1003-6326(15)63765-7
22. Ashby, M.F.: A first report on deformation-mechanism maps. Acta Metall. **20**(7), 887–897 (1972). https://doi.org/10.1016/0001-6160(72)90082-X
23. Maurya, A.K., Yeom, J.T., Kang, S.W., Park, C.H., Hong, J.K., Reddy, N.S.: Optimization of hybrid manufacturing process combining forging and wire-arc additive manufactured Ti-6Al-4V through hot deformation characterization. J. Alloys Compd. **894**, 162453 (2022). https://doi.org/10.1016/j.jallcom.2021.162453
24. Jenab, A., Taheri, A.K., Jenab, K.: The Use of ANN to Predict the Hot Deformation Behavior of AA7075 at Low Strain Rates, vol. 22, no. March, pp. 903–910, (2013). https://doi.org/10.1007/s11665-012-0332-y
25. Karimzadeh, M., Malekan, M., Mirzadeh, H., Saini, N., Li, L.: Hot deformation behavior analysis of as-cast CoCrFeNi high entropy alloy using Arrhenius-type and artificial neural network models. Intermetallics. **168** (February, 2024). https://doi.org/10.1016/j.intermet.2024.108240
26. Jalham, I.S.: Modeling capability of the artificial neural network (ANN) to predict the effect of the hot deformation parameters on the strength of Al-base metal matrix composites. Compos. Sci. Technol. **63**(1), 63–67 (2003). https://doi.org/10.1016/S0266-3538(02)00176-8
27. Shu, X.: A comparative study on constitutive equations and arti Fi Cial neural network model to predict high-temperature

deformation behavior in nitinol 60 shape memory alloy, (2015). https://doi.org/10.1557/jmr.2015.144
28. Xiao, X., Liu, G., Hu, B., Zheng, X., Wang, L., Chen, S.: Ullah.,A comparative study on Arrhenius-type constitutive equations and artificial neural network model to predict high-temperature deformation behaviour in 12Cr3WV steel. Comput. Mater. Sci. **62**, 227–234 (2012). https://doi.org/10.1016/j.commatsci.2012.05.053
29. Kishor, B., Chaudhari, G.P., Nath, S.K.: Hot deformation characteristics of 13Cr-4Ni stainless steel using constitutive equation and processing map. J. Mater. Eng. Perform. **25**(7), 2651–2660 (2016). https://doi.org/10.1007/s11665-016-2159-4
30. Kumar, S., Karmakar, A., Nath, S.K.: Construction of hot deformation processing maps for 9Cr-1Mo steel through conventional and ANN approach, *Mater. Today Commun.*, vol. 26, no. November p. 101903, 2021, (2020). https://doi.org/10.1016/j.mtcomm.2020.101903
31. Zhu, L., He, J., Zhang, Y.: A two-stage constitutive model of X12CrMoWVNbN10-1-1 steel during elevated temperature. Mater. Res. Express. **5**(2), 1–11 (2018). https://doi.org/10.1088/2053-1591/aaa911
32. McQueen, H.J., Ryan, N.D.: Constitutive analysis in hot working. Mater. Sci. Eng. A. **322**, 1–2 (2002). https://doi.org/10.1016/S0921-5093(01)01117-0
33. Laasraoui, A., Jonas, J.J.: Prediction of steel flow stresses at high temperatures and strain rates. Metall. Trans. A. **22**(7), 1545–1558 (1991). https://doi.org/10.1007/BF02667368
34. Oudin, A., Barnett, M.R., Hodgson, P.D.: Grain size effect on the warm deformation behaviour of a Ti-IF steel. Mater. Sci. Eng. A. **367**, 1–2 (2004). https://doi.org/10.1016/j.msea.2003.10.273
35. Jonas, J.J., Quelennec, X., Jiang, L., Martin, É.: The avrami kinetics of dynamic recrystallization. Acta Mater. **57**(9), 2748–2756 (2009). https://doi.org/10.1016/j.actamat.2009.02.033
36. Mirzadeh, H., Parsa, M.H., Ohadi, D.: Hot deformation behavior of austenitic stainless steel for a wide range of initial grain size. Mater. Sci. Eng. A. **569**, 54–60 (2013). https://doi.org/10.1016/j.msea.2013.01.050
37. Rasti, J., Meratian, M., Najafizadeh, A.: Application of the Taguchi approach to investigate the softening kinetics of AISI 304 stainless steel during hot deformation. Int. J. Mater. Res. **102**(8), 1053–1060 (2011). https://doi.org/10.3139/146.110457
38. Marchattiwar, A., Sarkar, A., Chakravartty, J.K., Kashyap, B.P.: Dynamic recrystallization during hot deformation of 304 austenitic stainless steel. J. Mater. Eng. Perform. **22**(8), 2168–2175 (2013). https://doi.org/10.1007/s11665-013-0496-0
39. Hu, M., Dong, L., Zhang, Z., Lei, X., Yang, R., Sha, Y.: Correction of flow curves and constitutive modelling of a Ti-6Al-4V alloy. Met. (Basel). **8**(4), 256 (2018). https://doi.org/10.3390/met8040256
40. Cai, J., Li, F., Liu, T., Chen, B., He, M.: Constitutive equations for elevated temperature flow stress of Ti-6Al-4V alloy considering the effect of strain. Mater. Des. **32**(3), 1144–1151 (2011). https://doi.org/10.1016/j.matdes.2010.11.004
41. Haghdadi, N., Zarei-Hanzaki, A., Khalesian, A.R., Abedi, H.R.: Artificial neural network modeling to predict the hot deformation behavior of an A356 aluminum alloy. Mater. Des. **49**, 386–391 (2013). https://doi.org/10.1016/j.matdes.2012.12.082
42. Yang, Z.N., Dai, L.Q., Chu, C.H., Zhang, F.C., Wang, L.W., Xiao, A.P.: Effect of aluminum alloying on the hot deformation behavior of Nano-bainite bearing steel. J. Mater. Eng. Perform. **26**(12), 5954–5962 (2017). https://doi.org/10.1007/s11665-017-3018-7
43. He, A., Xie, G., Zhang, H., Wang, X.: A comparative study on Johnson-Cook, modified Johnson-Cook and Arrhenius-type constitutive models to predict the high temperature flow stress in 20CrMo alloy steel. Mater. Des. **52**, 677–685 (2013). https://doi.org/10.1016/j.matdes.2013.06.010